Compatibility of Chlorinated Polyolefin with the Components of Thermoplastic Polyolefin: A Study by Laser Scanning Confocal Fluorescence Microscopy

Yuechun Ma, J. P. S. Farinha,† and Mitchell A. Winnik*

Department of Chemistry, University of Toronto, 80 St. George Street, Toronto, Ontario, Canada M5S 3H6

Phillip V. Yaneff

E.I. DuPont Canada, 408 Fairall Street, Ajax, Ontario, Canada L1S 1R6

Rose A. Ryntz

Visteon Automotive Systems, Dearborn, Michigan 58121

Received July 11, 2003; Revised Manuscript Received May 3, 2004

ABSTRACT: Dye-labeled samples of a chlorinated (21.8 wt % Cl), maleated polypropylene (CPO), and a dye-labeled sample of poly(ethylene-*co*-butene) (EBR28, with 28 wt % butene) were synthesized and characterized. The dye was a functional benzothioxanthene related to the commercial dye Hostasol Yellow 3G. These substances were introduced as tracers into blends of CPO with polypropylene (PP) and with EBR9 (9 wt % butene) as well as ternary blends of CPO + PP + EBR9. The morphology of the blends was examined by laser scanning confocal fluorescence microscopy. Control experiments at 5 wt % tracer showed that the dye-labeled CPO was fully miscible with its unlabeled precursor and that dye-labeled EBR28 was fully miscible with pure EBR9. The blend experiments showed that this particular CPO was much more miscible with EBR9 than with PP. Ternary blend experiments intended to mimic the composition of a thermoplastic polyolefin (TPO, with 25% EBR9 as the impact modifier) showed that the EBR formed micron size droplets in the PP matrix and that the CPO completely engulfed the EBR droplets to form a core−shell morphology. Center cross sections of these droplets showed the CPO layer to be uniform in thickness, with a sharp interface with the PP matrix. The inner interface, between the CPO and EBR, was noticeably broader, with a thickness on the order of 0.5 μm, indicating only weak segregation between these two components of the blend.

Introduction

The term TPO (thermoplastic polyolefin) refers to a family of polyolefin blends consisting of impact modified polypropylene (PP) with various other polyolefins as the dispersed phase. Common examples for the impact modifier are ethylene−propylene rubber (EPR) and ethylene−butene rubber (EBR) of various compositions. This type of polymer is widely used for the fabrication of plastic automobile parts such as bumpers and fascia. These parts normally need to be painted. Because of the low surface energy of TPO, there is serious problem of paint adhesion to the plastic part. To promote adhesion, injection molded TPO parts are commonly coated with an adhesion promoter consisting of a maleated, chlorinated polyolefin referred to generically as CPO. While CPO technology has evolved over the past several years as manufacturers have learned to prepare polymers of higher purity and better-defined molar mass and molar mass distribution, the performance level of CPO-coated TPO as a substrate for automotive base coat is far from optimum. Within the automotive industry, there is a hope that if one had a better understanding of the mechanism of CPO adhesion to TPO and how the strength of adhesion depends on processing conditions, one could use this knowledge to design better coatings.

This has been the motivation for a number of studies that investigated the interaction between CPOs and TPOs.[1−10] Among the variables in these investigations were the choice of organic solvent for coating the CPO onto the TPO,[2] the morphology of the TPO substrate,[8,11,12] and the subsequent baking conditions of the coated part.[3] What is also important to recognize is that there are many different CPOs available in the commercial marketplace. Even for CPOs that are based on a polypropylene (PP) backbone, they differ in the chlorine content, mean molar mass, and degree of substitution by succinic anhydride groups. Product literature in this field suggests that polypropylene-based CPOs with low levels of chlorine content (18, 20 wt % Cl) provide better adhesion to high-modulus (i.e., highly crystalline isotactic) PP-based TPO than CPOs with a higher Cl content.

A number of hypotheses have been put forward to explain CPO adhesion to TPO. Among the most interesting is the idea that solvent promotes CPO penetration into TPO (either the atactic PP component of the PP itself or the impact modifier).[1−6] Either entanglement or resistance to chain pullout[10,13] provides the adhesive strength.

In this paper, we are interested in assessing the miscibility and compatibility of the components of a high-modulus TPO with a relatively well-defined CPO. The PP component is a commercial isotactic PP of high crystallinity prepared by Ziegler−Natta polymerization, whereas the impact modifier is an ethylene−butene

† Permanent address: Centro de Quimica Fisica Molecular, Instituto Superior Tecnico, Av Rovisco Pais, 1049-001 Lisbon, Portugal.

* To whom correspondence should be addressed: e-mail mwinnik@chem.utoronto.ca.

10.1021/ma030381b CCC: $27.50
Published on Web 07/29/2004

copolymer with 9 mol % butene groups. The CPO we examine has a low chlorine content (21.8 wt %) and is intended to be used with this particular type of TPO. While traditional studies of CPO interaction with TPO involve coating the CPO onto a premolded TPO substrate, in this report we describe a different approach. We examine the morphology of blends of the CPO with the individual TPO components and then with the TPO blend. To obtain contrast, a small fraction of the CPO is labeled with a fluorescent dye. In the blends, the dye renders the CPO phase visible in laser confocal fluorescence microscopy measurements.[14−18] As a control, some experiments were carried out in which a dye-labeled EBR is added to the EBR[15,18] component in experiments carried out with unlabeled CPO.

Through these experiments, we learn that the CPO is strongly immiscible with PP and partially miscible with this particular EBR. In an annealed three-component blend, the CPO wets the EBR droplets to give a core−shell structure.

Experimental Section

Materials. Isotactic polypropylene (PP1042) and ethylene−butene rubber (Exact 3125) with 9 wt % butene were obtained from Exxon. Dye-labeled EBR was prepared from a maleated EBR (MEBR, Fusabond N MO-524D) from Du Pont Canada. This sample was prepared by maleation of a metallocene EBR (Exxon) containing 28 wt % butene. The CPO sample, a chlorinated maleated polypropylene (Superchlon 872S, Japan Paper Industries Ltd.), contains 21.8 wt % Cl (manufacturer's specification). A sample was purified by dissolving the polymer in refluxing xylene and then precipitating the polymer by pouring the hot xylene solution slowly into a large excess of cold methanol, followed by drying, first in air and then under vacuum. We determined the anhydride content by hydrolysis of the anhydride group to carboxylic acid groups, followed by anhydrous acid−base titration[19] with a 0.0217 N methanolic KOH solution. The anhydride content was 0.19 mmol/g polymer for the raw CPO sample and 0.12 mmol/g for the purified sample. The anhydride content of MEBR, determined similarly, was 0.060 mmol/g polymer.

Synthesis of Dye-Labeled CPO. The synthesis and characterization of the aminohexyl benzothioxanthene fluorescent dye HY-6-NH_2 is described elsewhere.[15] Samples of MEBR and CPO were labeled with HY-6-NH_2 through reactions with their respective anhydride substituents. The reactions were carried out under similar conditions, with only variation in the amount of HY-6-NH_2 used according to the anhydride content of each polymer. A typical labeling reaction procedure for CPO is as follows. Purified CPO (8 g) was dissolved in xylenes (400 mL) in the presence of molecular sieves (3 g). The mixture was heated to reflux with stirring under a N_2 atmosphere. Reflux was kept for 2 h in order to remove possible water from the system before the introduction of HY-6-NH_2 (0.48 g, 1.25×10^{-3} mol). The reflux was continued for 6 h, and then the hot solution was poured into excess methanol (4 L) at room temperature. The dye-labeled polymer was obtained by filtration. To remove the free dye retained in labeled polymer, the sample was dissolved in hot xylenes (2 wt % polymer), and then the hot solution was again poured into excess methanol. This process was repeated until no free dye was detected (UV−vis monitor) at low molar mass by gel permeation chromatography (GPC). The purified product was dried at 50 °C under vacuum overnight. Dye-labeled samples of MEBR and CPO are referred to as MEBR-HY and CPO-HY, respectively. GPC and FT-IR measurements indicated that fluorescent dye HY-6-NH_2 was chemically attached to polymers. GPC measurement also showed, for both MEBR and CPO, that the molecular weight of the polymer did not change significantly after the labeling reaction. We performed UV−vis spectroscopy to measure the dye incorporation to polymers by using Hostalsol Yellow-3G (HY-3G, Clariant) as a model compound ($\lambda_{max} = 456$ nm, $\epsilon = 1.83 \times 10^4$ in toluene). The dye incorporation into CPO-HY was 0.08 mmol/g polymer (3.2 wt %) while the dye incorporation into EBR-HY was 0.036 mmol/g polymer (1.4 wt % of HY-6-NH_2).

Polymer Blends Preparation. All polymer blends were prepared by solution precipitation, with the soluble polymer present at 2 wt %. In a typical preparation, a mixture of polymers (1 g) in the desired blend ratio was added to xylenes (50 mL), and the polymer solution was heated to reflux with stirring. After polymer dissolution was complete, the solution was poured into excess methanol/acetone mixture (50/50 v/v) with strong stirring. The precipitate was filtered, briefly air-dried for 6 h, and then dried in a vacuum oven at 60 °C overnight.

Molding and Annealing of Blends. We prepared films of each polymer blend by compression-molding the polymer blend in a Carver press. To prepare films, a small amount of blend (30−50 mg) was placed between two pieces of poly(ethylene terephthalate) (Melinex, PET) film. Two preheated stainless steel plates were used to hold the PET sandwiched powder. The assembly was set into the Carver press subjected to 4 metric tons pressure for 60 s at 120−160 °C, depending on the composition of the blend. To minimize the influence of postpressing thermal history, the pressed sample was quenched into cold water immediately after pressing. The thickness of pressed films was in the range 30−70 μm.

A small piece of polymer film was cut and sandwiched between two pieces of PET sheet. The PET sandwich was wrapped with aluminum foil, and then the aluminum foil set was inserted between two preheated stainless steel plates as quickly as possible. The whole set was annealed at 180 °C under vacuum for different periods of time. The annealed sample was quenched into cold water immediately after annealing to maintain the morphology.

Confocal Microscopy. Laser scanning confocal fluorescent microscopy (LSCFM) measurements were performed on a Zeiss LSM510 apparatus. An argon ion laser generates the excitation light ($\lambda_{ex} = 488$ nm). With a band-pass filter, we collected the emission light from the sample over the range of $\lambda_{em} = 505-550$ nm. The pinhole was set at 100 μm, resulting in a focal plane less than 0.8 μm thick. Optical sections were obtained at various distances from the film surface by moving the focal plane along the *z*-direction, resulting in a series of images. The film surface was defined as the film−air interface. The "find" function of the operating program was used to get satisfactory images by automatically adjusting the gain and the discrimination of the instrument. To ensure that the morphology examined was typical of the film as a whole, at least two different regions were imaged to obtain a *z*-section scan.

Image Analysis. Image analysis was carried out on LSCFM images of annealed PP/EBR/CPO blends, in which MEBR-HY was the tracer. In some experiments involving HY-labeled CPO, information was obtained on the raw images collected by the microscope. Through *z*-sectioning, center cuts of individual isolated droplets were identified. Profiles of fluorescence intensity across the PP/CPO and CPO/EBR interfaces were obtained by measuring intensities along lines drawn across the CPO shell that passed through the center of the EBR droplet. To obtain reliable statistics, we examined 20 droplets with a minimum of four lines per droplet. For each line, we calculated the full width at half-maximum (fwhm) of the fluorescence intensity peak corresponding to the CPO shell surrounding the EBR droplet. In addition, we calculated the individual widths on the PP and EBR sides of the peak maximum.

In other experiments with HY-labeled EBR, in which we attempted to quantify the droplet size and shape distribution, the images were subjected to Gaussian filtering and binarization before being analyzed with an image analysis program. The Gaussian filter function of Photoshop software was chosen to average the fluorescence intensity for images taken at different distances from the film surface and to compensate for intensity fluctuations resulting from light scattering or other artifacts. The Gaussian values were 25

pixels for PP/EBR/CPO blend annealed at 180 °C for 100 min and 30 pixels for the sample annealed for 300 min. The background was inverted and multiplied by the original image to obtain the corrected image, which therefore presents a normalized range of intensity levels. The normalized image was then binarized by adjusting the threshold to a value at the midpoint between the smaller and larger peaks of the intensity level histogram. (The smaller peak corresponds to the fluorescent objects and the larger peak to the background.) The threshold level was not equal for all images because the normalization through Gaussian filtering is not perfect, and therefore the levels of the histogram peak do not appear at exactly the same values in all images. This variation is not problematic if one uses the same relative position (i.e., the minimum point between the peaks) in the intensity level histogram of each image. The binarized image was treated with a noise-smoothing function (Photoshop) in order to eliminate isolated pixels (from binarization noise). Each image was then inspected visually to ensure that no significant image distortion had taken place. In this process, a thin colored perimeter line was generated through the image analysis software around each of the objects in the filtered, binarized image. An image of this ensemble of perimeter lines was then superimposed onto the original image to test whether each of the bright areas in the original image (see Figure 9) was faithfully reproduced in the binarized image. Unlike the human eye, the image analysis software does not recognize touching areas in the binarized image as due to separate droplets. We used Photoshop software to cut aggregated objects in each image into separate areas prior to image analysis. Each binarized image was then analyzed with AIS image workstation software developed by Imaging Research Inc. (St. Catherines, ON) to obtain the number, diameter, and form factor of the cross sections in each image. The total fluorescence area in each binarized image was also calculated.

Results and Discussion

Synthesis of Dye-Labeled Polymers. We prepared dye-labeled samples of CPO and EBR. CPO is intended to function as an adhesion promoter to TPO blends. In this function, the chlorinated backbone is thought to enhance adhesion to the polyolefin, whereas the anhydride groups promote interaction with the basecoat used to paint the polymer part. The CPO of interest contained 0.19 mmol/g of succinic anhydride group. The MEBR sample we employed was a maleated form of a metallocene EBR containing 28 wt % butene. Its anhydride content was found to be 0.060 mmol/g polymer. These samples were reacted with a limiting amount of the functional dye HY-6-NH_2. The dye content of the purified dye-labeled polymers is 0.08 mmol/g polymer for CPO-HY and 0.036 mmol/g polymer for EBR-HY.

Miscibility of Dye-Labeled Polymer with Its Starting Material. In designing these experiments, we were concerned that the presence of the dye on CPO-HY might perturb its interactions with other components of a blend. To minimize this effect, we wished to use the dye-labeled CPO as a tracer in the original CPO. To use the dye-labeled polymer as a tracer for understanding the compatibility of CPO with the components of TPO, the dye-labeled polymer has to meet three criteria. First, the dye-labeled polymer must be completely miscible with its precursor polymer. Second, the introduction of dye-labeled polymer into starting material should not change the nature of original material. Finally, the dye-labeled polymer, in trace amounts, has to give sufficient optical contrast in fluorescence microscopy experiments. Guided by these criteria, we prepared a 95:5 CPO/CPO-HY blend as described in the Experimental Section. The compression-molded film was annealed at 180 °C under vacuum for 300 min, followed by quenching the annealed film into cold water to freeze the morphology developed through annealing. Both annealed and nonannealed films were examined by LSCFM.[20]

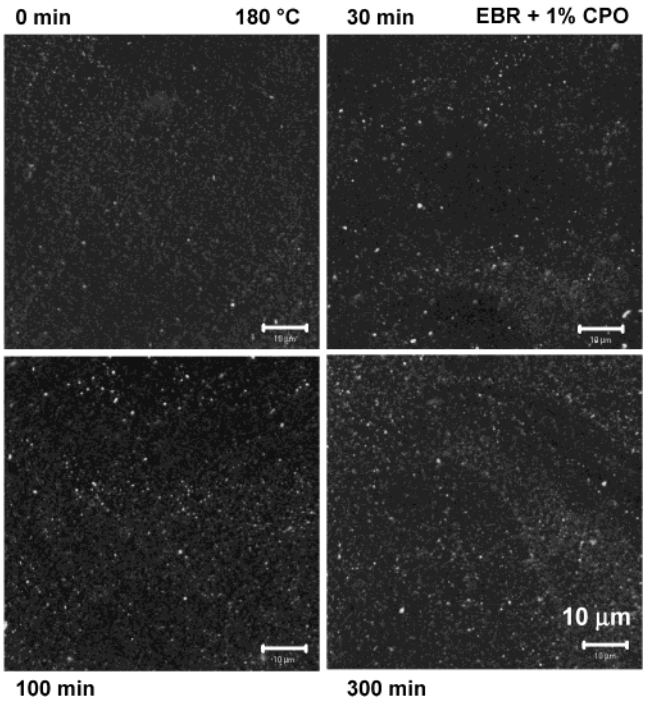

Figure 1. Morphology evolution of films of a blend of 99/1 EBR/CPO annealed at 180 °C for various times. Scale bars are 10 μm. Background fluorescence is seen in all images, indicating the presence of CPO-HY in the matrix. The bright spots are due to regions rich in CPO-HY.

Images of 95/5 CPO/CPO-HY as prepared and annealed at 180 °C for 300 min were compared (not shown). These images were featureless: uniformly distributed fluorescence was observed for both samples. No phase separation between the CPO matrix and the dissolved CPO-HY polymer could be detected. The result indicates that CPO-HY is completely miscible with its original precursor when present at the ratio of 5:95 by weight. This blend was used as the CPO component in all measurements described here. We also prepared a blend of MEBR-HY with EBR9 in a weight ratio of 5:95. In this sample, MEBR-HY serves as a tracer for EBR9. Here one might expect problems with sample miscibility since the main component of the blend is an EBR with 9 wt % butene, whereas EBR-HY is prepared from a less crystalline EBR with 28 wt % butene. Moffitt in our group has examined this system in detail and concluded that for this composition the two polymers are fully miscible.[15]

CPO Blends with EBR and PP. Morphology of EBR/CPO Blends. To study the compatibility of CPO with EBR, two blends of EBR and CPO were prepared by solution precipitation. These blends had composition ratios EBR:CPO of 99:1 and 98:2 by weight. In these experiments, the EBR was unlabeled and the CPO contained 5 wt % of CPO-HY as tracer. Compression-molded films were annealed at 180 °C under vacuum for various periods of time. Because phase separation and coarsening often evolve according to a power law behavior, we chose logarithmically spaced annealing times (0, 30, 100, and 300 min). A series of images of the 99:1 EBR/CPO sample annealed for different times are shown in Figure 1. For the film before annealing,

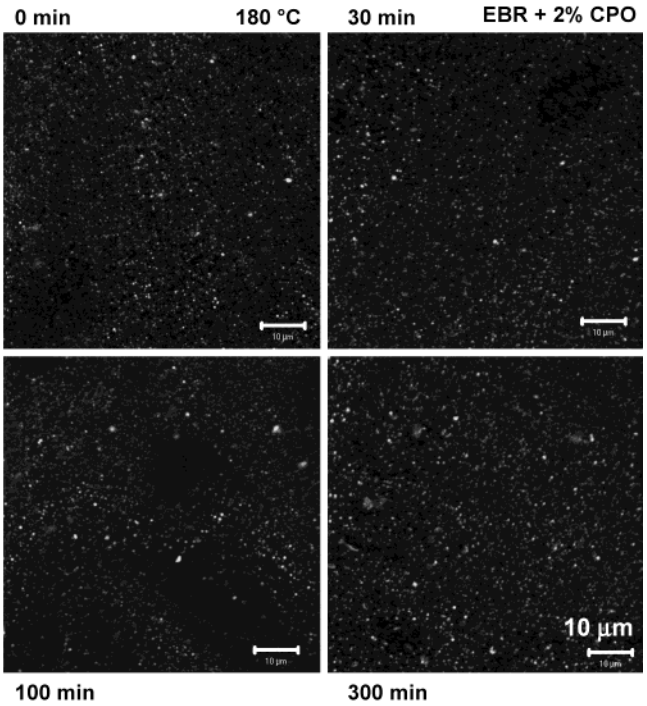

Figure 2. Morphology evolution of films of a blend of 98/2 EBR/CPO annealed at 180 °C for various times. Scale bars are 10 μm.

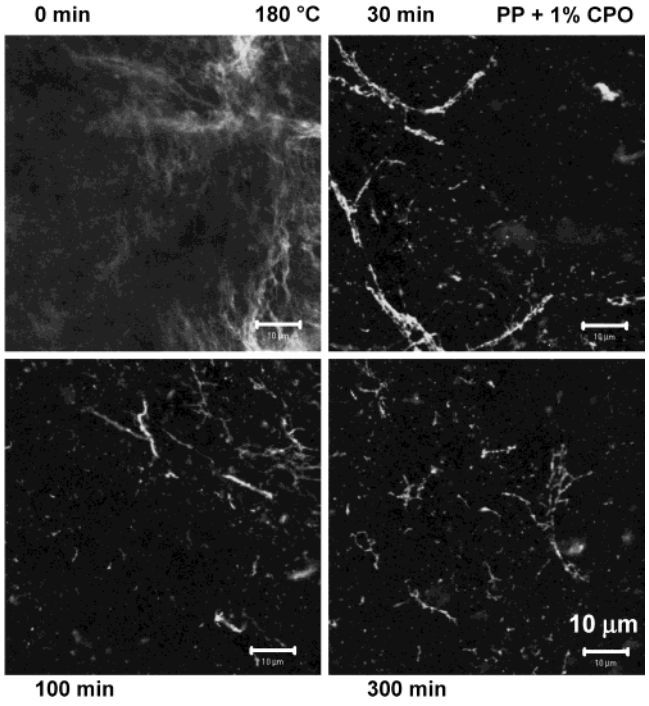

Figure 3. LSCFM images of films of a blend of 99/1 PP/CPO annealed at 180 °C for different times. Scale bars are 10 μm. The bright areas refer to CPO-rich domains.

we can see indications of phase separation that must have occurred during sample preparation. This effect may be related to the different solubility of the two polymers in the xylene/methanol/acetone mixture used to precipitate the polymer. We expect relatively little coarsening to occur during the rapid melt pressing of the sample at its molding temperature (120 °C).

The diameters of the bright CPO-rich domains in the nonannealed film are less than 1 μm. In addition, we observe strong background fluorescence in the EBR matrix. The contrast between bright domains and the background is not very sharp in this image, indicating the presence of CPO-rich domains too small to be resolved by optical microscopy. In the annealed samples, we note relatively small changes, characterized primarily by a slight increase in the number and size of the bright CPO-rich domains. We still can observe background fluorescence in these annealed samples, with poor contrast between bright CPO-rich domains and the EBR matrix. Images taken at different depths in the film (not shown) were very similar. These results may point to some miscibility between the two polymers and indicate that phase separation was far from complete even when the sample was annealed for 300 min.

To obtain more information on the compatibility of CPO with EBR, similar experiments were performed on a 98:2 EBR/CPO blend. Typical results are shown in Figure 2. At the higher CPO concentration in the blend, the samples without annealing show relatively dense CPO-rich domains in EBR matrix, but the size of the CPO domains is almost the same as those in Figure 1. As in the 99:1 EBR/CPO blend, the size and density of domains increased slightly upon annealing. Again, we observe substantial background fluorescence in the sample annealed for 300 min, suggesting the persistence of small CPO-rich domains dispersed in the EBR matrix or partial miscibility of CPO with EBR at this composition.

Morphology of PP/CPO Blends. To compare experiments with polypropylene with those with EBR, we prepared sample blends with a similar composition ratio, PP:CPO = 99:1 and 98:2 by weight. Films of these two PP/CPO blends were compression-molded at 160 °C under 4 metric tons pressure for 60 s. In Figure 3 we show LCFM images of morphology development in these films. In the compression-molded film without annealing containing 1% CPO, we see bright phases with irregular shapes. A series of *z*-section images were taken on the sample before annealing by moving the focus along the *z*-direction at 1 μm intervals between two consecutive optical slices. The *z*-stack of images showed anisotropic CPO distribution not only along the *z*-direction but also within each $x-y$ plane. This morphology may be related to more rapid precipitation and crystallization of the PP component during precipitation into the acetone–methanol mixture.

The films were then annealed at 180 °C under vacuum for 30, 100, and 300 min. With annealing, we found that the CPO phase started to aggregate and form wormlike structures and clusters. The CPO did not form spherical domains in this PP/CPO blend, as we observed in EBR/CPO blends. After annealing the samples, the contrast between the bright CPO phase and the dark PP background became much sharper than that of EBR/CPO blends. Through *z*-section imaging, we found that CPO formed a network in some CPO-rich regions of the film, whereas in other regions of the film, the CPO concentration was very low. Upon extended annealing (300 min), we observed a more obvious network formed in discrete locations in the film, with other regions depleted of CPO. This effect is reminiscent of phase coarsening by hydrodynamic flow through a network of fine channels in the blend.[21] Similar experiments were carried out on a 98:2 PP/CPO blend. As shown in Figure 4, a similar morphology was obtained. The only difference is a higher density of bright spots associated with the higher concentration of CPO in this blend.

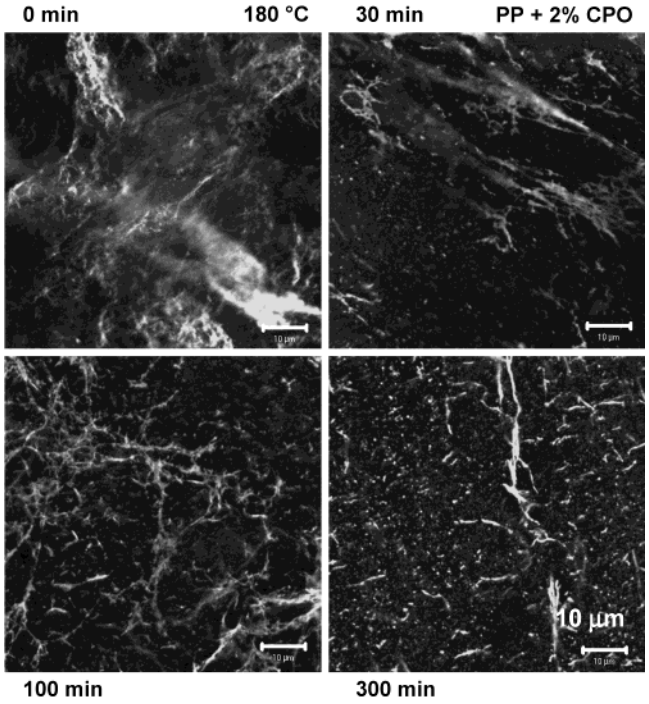

Figure 4. LSCFM images of films of a blend of 98/2 PP/CPO annealed at 180 °C for different times. Scale bars are 10 μm. The bright areas refer to CPO-rich domains.

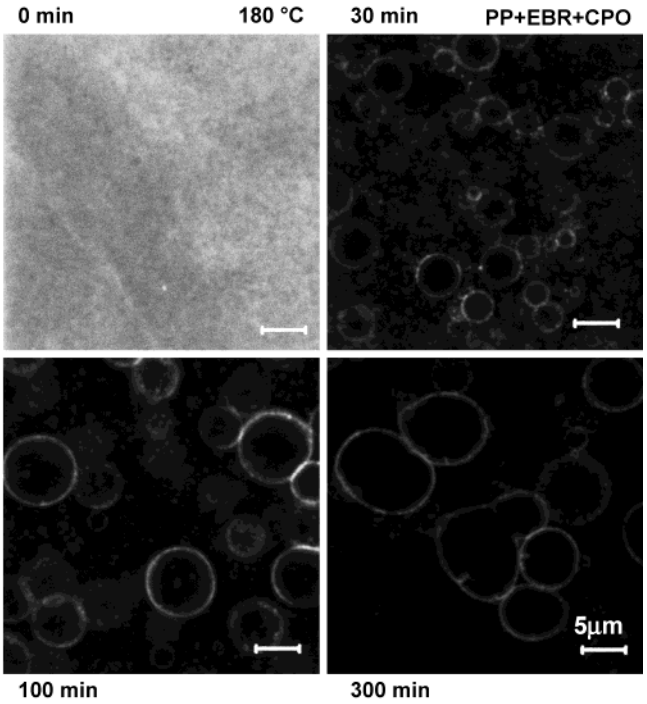

Figure 5. Morphology evolution of films of a ternary blend consisting of 74/23.5/2.5 PP/EBR/CPO in which the CPO contains CPO-HY. The films were annealed at 180 °C for different times. Scale bars are 5 μm. All images were taken about 5 μm under the film surface.

CPO Blends with PP + EBR. TPO consists of a blend of polypropylene with a second polyolefin, here EBR. A typical blend ratio is 75% PP and 25% impact modifier. CPO is used to coat injection-molded samples of this blend. To test the interaction of CPO with the TPO components, we prepared ternary blends of CPO with PP + EBR. These blends had the composition 74/23.5/2.5 PP/EBR/CPO by weight, in which one of the components (CPO or EBR) contained a dye-labeled polymer as a tracer. Figure 5 shows LSCFM images of one such blend in which the CPO component is fluorescent. The initial film shows few features at all depths, consistent with domains too small to be resolved. Upon annealing at 180 °C, the structure evolved through phase coarsening. One observes droplets, which we show below to consist of EBR, each surrounded by a fluorescent ring. These images suggest that the CPO component engulfs droplets of EBR in the blend. This fascinating result is consistent with the observations described above that the CPO is more compatible with EBR than with PP.

For the samples annealed for 30 and 100 min, some small bright CPO domains are visible in the background. In some EBR droplets small CPO particles are also seen. The small size of the core−shell structures and the small bright CPO domains in the background suggest that phase separation is still at an early stage. After 300 min annealing time, the size of core−shell droplets increased while their number decreased. In addition, we no longer see small bright CPO domains in the PP phase. Comparing the three annealed samples, we find that the thickness of the CPO layer at the PP/CPO interface does not change dramatically. Visually, the interface between the CPO ring and the surrounding PP appears sharper than the interface between the CPO and the interior EBR phase, especially for the sample annealed for 100 min.

To emphasize the core−shell nature of these droplets, we present a *z*-stack of images in Figure 6. This set of images with enhanced magnification was taken from a sample annealed for 300 min. Each image represents an 18.3 × 18.3 μm slice of the film, with 0.25 μm separating each image. From the image with the largest circle, we estimate that the diameter of the EBR core is about 9 μm and the thickness of CPO shell is about 1 μm.

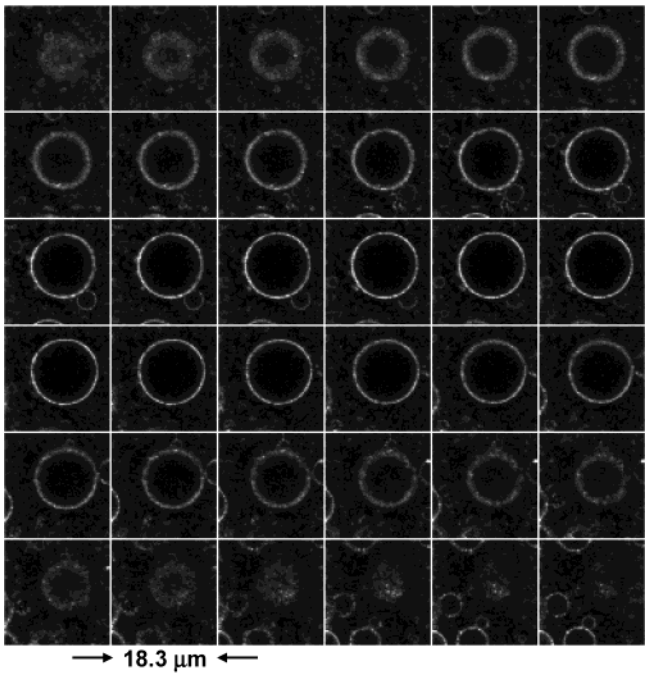

Figure 6. *Z*-section stack of images of a single EBR/CPO spherical core−shell-like particle from the sample shown in Figure 5 (annealed 300 min). The size of each image window is 18.3 μm × 18.3 μm. The depth interval between two consecutive images is 0.25 μm.

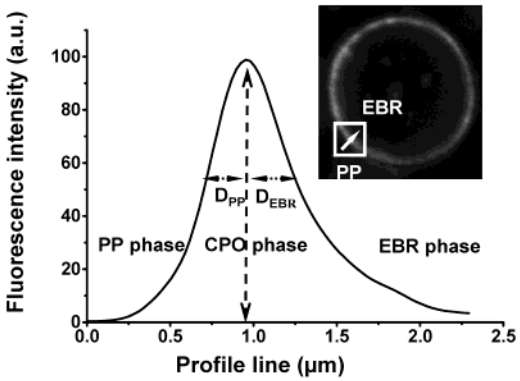

Figure 7. Profile of the fluorescence intensity across the CPO shell (across the PP/CPO/EBR interfaces) at the center of an EBR−CPO core−shell particle. This trace is taken as shown in the inset from the 8 μm diameter circular particle in the lower center of Figure 5 (100 min annealing). To obtain meaningful values of D_{PP} and D_{EBR}, we analyzed four lines each drawn to bisect center cross sections of 20 droplets, both for samples annealed 100 min and those annealed 300 min at 180 °C.

Figure 7 shows the profile of fluorescence intensity across a CPO ring in a center section of a CPO-coated EBR droplet like those shown in Figures 5 and 6. The profile is taken along a line perpendicular to the tangent to the circle and passes through the center of the droplet. The profile shown is taken along the line shown by the arrow in the inset to the figure. One can see the asymmetric nature of the profile, which is broader on the EBR side of the peak maximum than on the PP side. To analyze this profile, we assume that the PP−CPO interface is sharp and consider the breadth of the peak to the PP side of the peak maximum at 50% intensity (D_{PP}) to be an indication of the optical resolution of the microscope. From center sections of 40 droplets (20 from samples annealed 100 min and 20 from samples annealed 300 min) examined at four locations each, we found $D_{PP} = 0.36 \pm 0.03$ with no difference between annealing conditions. From the corresponding EBR sides of the profiles, we found $D_{EBR} = 0.48 \pm 0.04$ μm for samples annealed for 100 min and $D_{EBR} = 0.45 \pm 0.03$ μm for samples annealed for 300 min. While these values are close to the resolution limit of the confocal microscope, the difference is significant. This result points to the much weaker segregation between CPO and EBR compared to CPO and PP.

Droplet Size Distribution in a 74/23.5/2.5 PP/EBR/CPO Blend. Another set of experiments were carried out with a blend similar to that shown in Figure 5 (74/23.5/2.5 PP/EBR/CPO by weight) in which the EBR component contained the fluorescent tracer. Images of the resulting blend are shown in Figure 8. These images show many structural similarities with those in Figure 5. The freshly molded film shows few features, whereas the films annealed for 100 and 300 min at 180 °C show the formation of spherical objects very similar in size to those seen in Figure 5. The importance of these images is that they confirm the composition of the droplets seen in experiments in which the CPO was labeled.

We initially expected a spatially uniform distribution of droplet sizes in the blends we prepared. Through depth profiling, we noticed certain features of the blend that suggested that this was not the case. For example, near the surface of films annealed for 100 min, and at 10−15 μm under the surface, we observed a relatively large number of small droplets that decreased significantly when the films were annealed for 300 min. Between these regions, at a depth of approximately 5 μm, many fewer particles were observed. Another observation, which is reflected in Figure 9, is that the EBR droplets near the surface appear to be larger than those deeper in the film.

To learn more about droplet distribution, we employ image analysis to examine blends similar to those shown in Figure 8 in which the EBR component contains the fluorescent dye. As described in the Experimental Section, image processing begins with Gaussian filtering of the images followed by binarization. Figure 9 shows the consequences of these steps on the images themselves. A useful test of image fidelity is a visual comparison of each filtered binarized images with its original images. We do not see significant changes in the features of the images before and after binarization. We further tested the binarization procedure by comparing images taken at different locations within the film. This comparison revealed difficulties in obtaining satisfactory contrast in images taken at locations deeper than 15 μm from the surface. Thus, images for image analysis were taken from the top 15 μm of the film. This process is sufficiently arduous that we carried out this analysis for a *z*-stack of 31 images (at 0.5 μm intervals) obtained from a single (hopefully typical) location on a film annealed for 100 min at 180 °C and for a second *z*-stack of images for a film annealed for 300 min.

From the binarized images, at each depth, the image analysis program counts the number of fluorescent objects and calculates other features of the image such as the fractional area represented by fluorescent objects. We also used the features of the program that calculate the circular diameter, which is the diameter of a circle whose area is equivalent to the area of the target, and the form factor, which is a standard estimate of circularity that relates perimeter length to area. This measurement varies from 0 to 1, with 1 being a perfect circle.

The results of this image analysis are presented in Figures 10 and 11, where the averages plotted in Figures 10B and 11A are number-averaged values. In Figure 10A, we plot the number density of cross sections as a function of the distance from the film surface. The values plotted are the absolute number of fluorescent objects at each depth from the film surface. Because most of the droplets are larger than the 0.5 μm interval between successive cross sections, there should be a correlation in the data for neighboring cross sections. We did not attempt any correction to account for the vertical dimensions of the droplets. We are looking for effects that appear at length scales on the order of or larger than the diameter of individual droplets. For samples annealed for both 100 and 300 min, the plot passes through a minimum 3−5 μm beneath the surface. This result reinforces our more qualitative observations described above.

In Figure 10B, we plot the average circular diameters of cross sections obtained at various depths from the film surface. Selective error bars are shown in the plot. These refer to the standard deviation of object sizes and not to the standard deviation of the mean. Because of the large distribution of object sizes in each image, these standard deviation values associated with each point are large. A better estimate of the reproducibility of the image analysis is the magnitude of adjacent points in

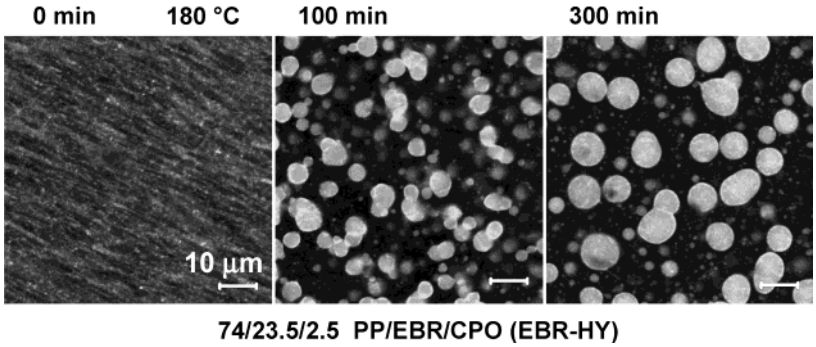

Figure 8. Morphology evolution of films of a ternary blend consisting of 74/23.5/2.5 PP/EBR/CPO in which the EBR component is labeled with the fluorescent dye; thus the bright areas are due to EBR. The size of each image window is 73 μm × 73 μm. The films were annealed at 180 °C for different times. Scale bars are 10 μm. All images were taken ca. 3 μm under the film surface.

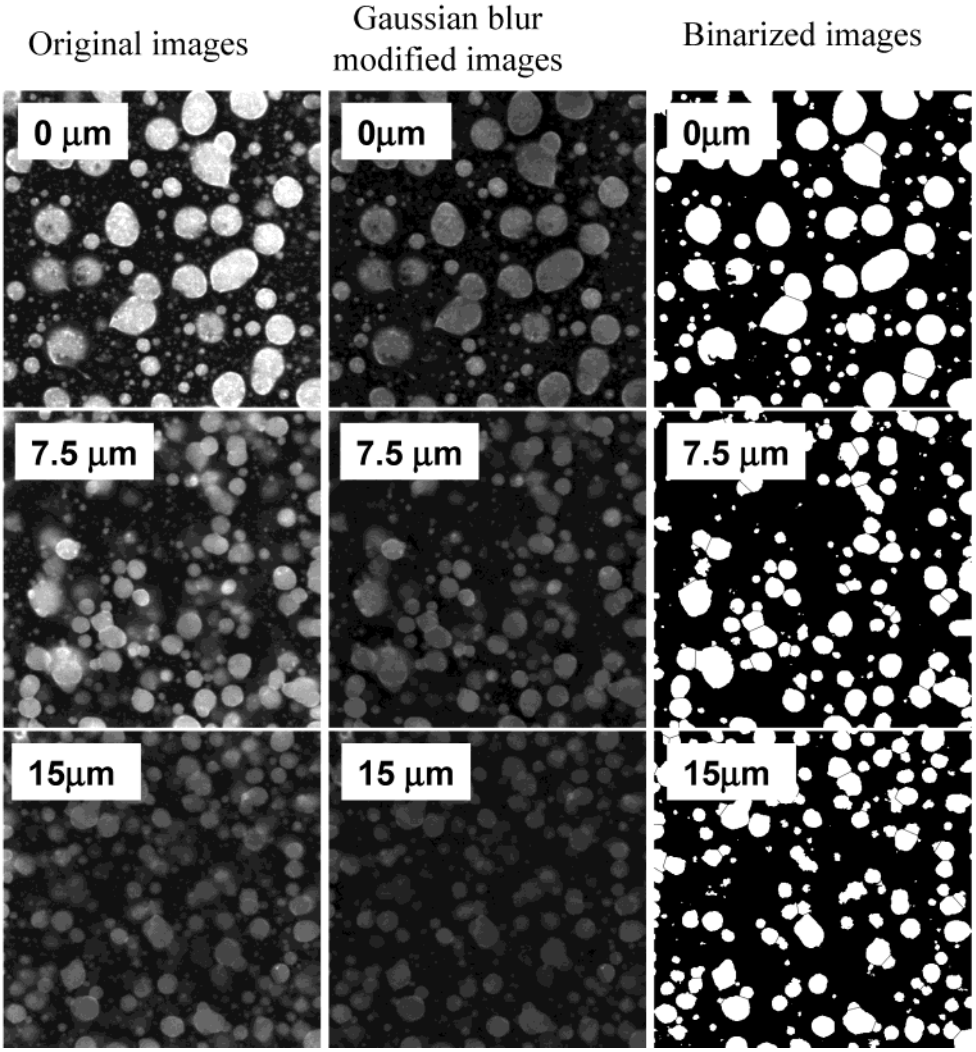

Figure 9. Image preparation procedure for image analysis. These samples of 74/23.5/2.5 PP/EBR/CPO with EBR-HY were annealed for 300 min at 180 °C (see Figure 8). The size of each image window is 73 μm × 73 μm. Left: original images captured at the film surface and 7.5 and 15 μm beneath the surface. Middle: the same images after Gaussian filtering with a setting of 30 pixels. The Gaussian value selected for the sample annealed at 180 °C for 100 min (image not shown) was 25 pixels. Right: the same images after binarization.

this plot. There is a strong suggestion in the plot that the cross-section diameters (and thus the droplet diameters) are smaller at depths greater than 10 μm below the surface than close to the surface.

Figure 11A shows the average form factor for all cross sections of droplets in each image against the distance from surface. The form factor is a measure of the spherical nature of an object, and average values in the range 0.85−0.9 indicate that the cross sections are nearly circular. Selective error bars are shown in the plot. The large standard deviation is in part an indication of the large distribution of shapes and in part an artifact of the way in which cross sections of aggregated droplets were treated. These were manually cut into separate areas using Photoshop software to delineate the separate nature of the particles. Cross-section areas

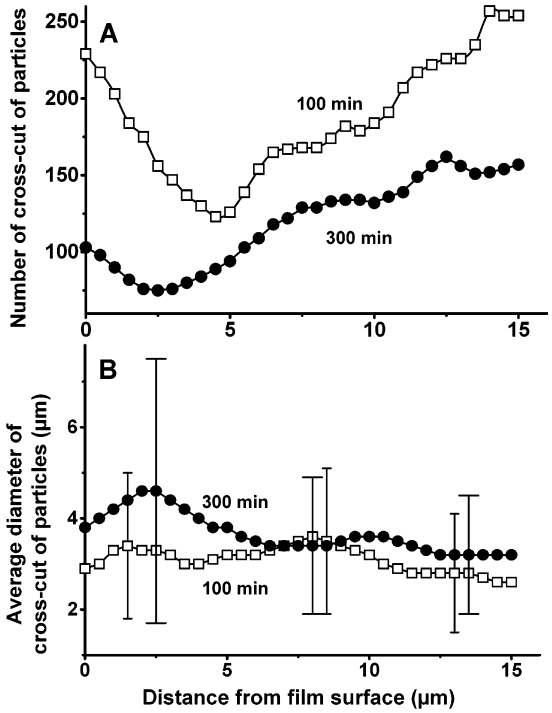

Figure 10. Results of analysis of the binarized images taken from the samples shown in Figure 8 annealed 100 and 300 min at 180 °C. (A) A plot of the number of cross sections of droplets in each image against the distance of the image from the film surface. (B) A plot of the average diameter of the droplets in each image against its distance from the film surface. The error bars do not refer to the standard deviation of the mean. Rather, they refer to one standard deviation from the mean of the diameters of the cross sections seen in the image. Each point in this figure and in Figure 11 represents data from a single micrograph. Thus, 31 images were analyzed for each sample.

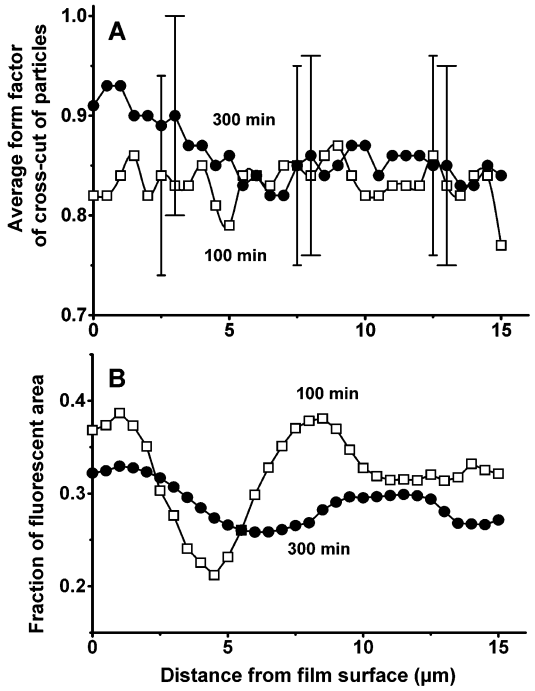

Figure 11. Results of analysis of the binarized images taken from the samples shown in Figure 8 annealed 100 and 300 min at 180 °C. (A) A plot of the average form factor of the cross sections of droplets in each image against its distance from the film surface for films. The error bars shown for selected data points refer to the one standard deviation for the variation in form factor for bright areas seen in the image at each depth. (B) A plot of the fractional fluorescence area in each images against its distance from the film surface.

cut in this way were less circular than those due to well-separated droplets. The larger values for cross sections near the film surface for the films annealed for 300 min indicate that these droplets tend to be somewhat more spherical than droplets at similar depths in the film annealed for 100 min. At depths below 6 μm, the form factor does not change significantly between 100 and 300 min annealing.

The blends under consideration consist of 24 vol % EBR and 2.4 vol % CPO. In the experiments described above, we learned that CPO is partially miscible with EBR but immiscible with PP. From this perspective, we anticipate that the volume fraction of fluorescent material in the blend consisting of EBR-HY + CPO will be 0.264. Thus, random cross sections through a matrix with a uniform distribution of CPO-coated EBR droplets should show a fractional fluorescent area of ca. 0.26.[22] The depth dependence of the fractional fluorescent areas of this blend, obtained from single sets of *z*-stacks at 100 and 300 min annealing, is presented in Figure 11B. Because the EBR component is labeled with the fluorescent dye, this plot should provide the best representation of the quantitative distribution of the EBR in the blend. Both plots are consistent with that in Figure 10A in suggesting a depletion of the EBR dispersed phase at distances between 4 and 8 μm below the surface. There is a sharp dip in the fraction of the fluorescent area in the range 3−5 μm below the surface for the 100 min sample. We cannot comment about whether this effect is general or reflects a fluctuation associated with the particular location of the film we chose to examine. This effect is less pronounced in the sample annealed for 300 min. The value of the fraction of fluorescent area averaged over the first 15 μm of the film is 0.32 for the sample annealed for 100 min and 0.29 for the sample annealed for 300 min. We conclude that both the CPO and EBR contribute to the fluorescent area of the binarized images and that there is a slight enrichment of the dispersed phase in the top 15 μm compared to its composition in the blend.

Summary

We described the synthesis and characterization of a dye-labeled chlorinated (21.8 wt % Cl), maleated polypropylene (CPO) and a dye-labeled sample of poly(ethylene-*co*-butene) (EBR28, with 28 wt % butene). The dye was a functional benzothioxanthene related to the commercial dye Hostasol Yellow 3G. These substances were introduced as tracers into blends of CPO with polypropylene (PP) and with EBR9 (9 wt % butene) as well as ternary blends of CPO + PP + EBR9. The morphology of the blends was examined by laser scanning confocal fluorescence microscopy (LSCFM). Control experiments at 5 wt % tracer showed that the dye-labeled CPO was fully miscible with its unlabeled precursor and that dye-labeled EBR28 was fully miscible with pure EBR9.

The blend experiments showed that this particular CPO was much more miscible with EBR9 than with PP. Ternary blend experiments intended to mimic the composition of a TPO (with 25% EBR as the impact modifier) showed that the EBR formed micron size droplets in the PP matrix and that the CPO completely engulfed the EBR droplets to form a core−shell morphology. From a sample annealed 100 min at 180 °C

and another annealed 300 min, a series of *z*-section images of 20 isolated droplets were taken. Center sections were analyzed to obtain a better understanding of the dimensions of the CPO shell. From intensity profiles taken across the CPO domains, we found that these shells were uniform in size, with a thickness on the order of 1 μm. The interface between CPO and PP was sharp (too small to resolve by optical microscopy) whereas a broader interphase, with a thickness on the order of 0.5 μm, was clearly evident between the CPO and EBR components.

Acknowledgment. The authors thank Materials and Manufacturing Ontario (MMO) and NSERC Canada for support of this research.

References and Notes

(1) Ryntz, R. A.; Prater, T. J.; Holubka, J. W. *J. Coat. Technol.* **1996**, *68* (857), 83.
(2) Ryntz, R. A.; Xie, Q.; Ramamurthy, A. C. *J. Coat. Technol.* **1995**, *67* (843), 45.
(3) Schmitz, P. J.; Holubka, J. W. *J. Adhes.* **1995**, *48*, 137.
(4) Tomasetti, E.; Legras, R.; Henri-Mazeaud, B.; Nysten, B. *Polymer* **2000**, *41*, 6597.
(5) Tomasetti, E.; Daoust, D.; Legras, R.; Bertrand, P.; Rouxhet, P. G. *J. Adhes. Sci. Technol.* **2001**, *15*, 13, 1589.
(6) Tomasetti, E.; Vandorpe, S.; Daoust, D.; Boxus, T.; Marchand-Brynaert, J.; Poleunis, C.; Bertrand, P.; Legras, R.; Rouxhet, P. G. *J. Adhes. Sci. Technol.* **2001**, *15*, 1589.
(7) Ryntz, R. A. *J. Coat. Technol.* **1991**, *63* (799), 63.
(8) Ryntz, R. A. *Prog. Org. Coat.* **1996**, *27*, 241.
(9) Ryntz, R. A.; Buzdon, B. *Prog. Org. Coat.* **1997**, *32*, 167.
(10) Ellis, T. S. *Polym. Eng. Sci.* **2001**, *41*, 2065.
(11) Morris, H. R.; Munroe, B.; Ryntz, R. A.; Treado, P. J. *Langmuir* **1998**, *14*, 2426.
(12) Morris, H. R.; Turner, J. F.; Munro, B.; Ryntz, R. A.; Treado, P. J. *Langmuir* **1999**, *15*, 2961.
(13) Raphael, E.; de Gennes, P. G. *J. Phys. Chem.* **1992**, *96*, 4002.
(14) Li, L.; Chen, L.; Bruin, P.; Winnik, M. A. *J. Polym. Sci., Part B: Polym. Phys.* **1997**, *35*, 979.
(15) Tong, J.; Moffitt, M.; Huang, X.; Winnik, M. A.; Ryntz, R. A. *J. Polym. Sci., Part A: Polym. Chem.* **2001**, *39*, 239.
(16) Li, L.; Sosnowski, S.; Kumacheva, E.; Winnik, M. A.; Rajaram, S.; Balke, S. T.; Chaffey, C. E. *Langmuir* **1996**, *12*, 2141.
(17) Li, L.; Sosnowski, S.; Chaffey, C. E.; Balke, S. T.; Winnik, M. A. *Langmuir* **1994**, *10*, 2495.
(18) (a) Moffitt, M.; Winnik, M. A. *J. Polym. Sci. Technol.* **2000**, *11*, 779. (b) Moffitt, M.; Rharbi, Y.; Li, H.; Chen, W.; Tong, J.; Winnik, M. A.; Thurman, D. K.; Oberhauser, J. P.; Kornfield, J. A.; Ryntz, R. A. *J. Polym. Sci., Part B: Polym. Phys.* **2002**, *40*, 2842.
(19) Sclavons, M.; Carlier, V.; De Roover, B.; Franquinet, P.; Devaux, J.; Legras, R. *J. Appl. Polym. Sci.* **1996**, *62*, 1205.
(20) Our CPO sample is stable to heating at 180 °C. GPC measurements on the original CPO sample and on the 95/5 CPO/CPO-HY blend baked at 180 °C in a vacuum oven for 300 min show no significant difference in molecular weight and molecular weight distribution. There is ca. 8% weight loss, which appears to be accompanied by interchain anhydride formation. Annealed CPO samples have poor solubility in THF but become completely soluble when a few drops of water are added to the THF.
(21) Moffitt, M.; Rharbi, Y.; Li, H.; Winnik, M. A. *Macromolecules* **2002**, *35*, 3321.
(22) Russ, J. C. *Practical Stereology*; Plenum Press: New York, 1986.

MA030381B